

# An allometry-based model of the survival strategies of hydraulic failure and carbon starvation

Pierre Gentine,<sup>1\*</sup> Marceau Guérin,<sup>2</sup> María Uriarte,<sup>3</sup> Nate G. McDowell<sup>4</sup> and Willam T. Pockman<sup>5</sup>

<sup>1</sup> Earth Institutes and Department of Earth and Environmental Engineering, Columbia University, 500 W 120<sup>th</sup> st., Office 842D, New York, NY 10027, USA

<sup>2</sup> Department of Earth and Environmental Engineering, Columbia University, New York, NY 10027, USA

<sup>3</sup> Department of Ecology and Evolutionary Biology, Columbia University, New York, NY 10027, USA

<sup>4</sup> Earth and Environmental Sciences, Los Alamos National Laboratory, Los Alamos, NM 87545, USA

<sup>5</sup> Department of Biology, University of New Mexico, Albuquerque, NM 87131, USA

## ABSTRACT

A simplified soil–plant–atmosphere–continuum model of carbon starvation and hydraulic failure is developed and tested against observations from a drought-manipulation experiment in a woodland dominated by piñon pine (*Pinus edulis*) and juniper (*Juniperus monosperma*) in New Mexico. The number of model parameters is reduced using allometric relationships. The model can represent more isohydric (piñon) and more anisohydric (juniper) responses. Analysis of the parameter space suggests four main controls on hydraulic failure and carbon starvation: xylem vulnerability curve, root:shoot area ratio, rooting depth and water use efficiency. For piñon, an intermediate optimal ( $1.5\text{--}2\text{ m}^2\text{ m}^{-2}$ ) tree leaf area index reduces the risk of hydraulic failure. For both piñons and junipers, hydraulic failure was relatively insensitive to root:shoot ratio across a range of tree LAI. Higher root:shoot ratios however strongly decreased the time to carbon starvation. The hydraulic safety margin of piñons is strongly diminished by large diurnal variations in xylem/leaf water potential. Diurnal drops of water potential are mitigated by high maximum hydraulic conductivity, high root:shoot ratio and stomatal regulation (more isohydric). The safety margin of junipers is not very sensitive to diurnal drops in water potential so that there is little benefit in stomatal regulation (more anisohydric). Narrower tracheid diameter and a narrower distribution of tracheid diameters reduce the risk of hydraulic failure and carbon starvation by reducing diurnal xylem water potential drop. Simulated tree diameter-dependent mortality varies between these two species, with piñon mortality decreasing with increasing tree size, whereas juniper mortality increases with tree size. Juvenile piñons might thus be overimpacted by water stress. Copyright © 2015 John Wiley & Sons, Ltd.

KEY WORDS cavitation; embolism; carbon starvation; physical model; allometry; tree diameter; isohydric anisohydric

Received 6 May 2014; Revised 9 March 2015; Accepted 28 May 2015

## INTRODUCTION

The sensitivity and resilience of terrestrial ecosystems to climate change are of growing research interest because of observations of increasing rates of drought-induced vegetation mortality (Allen *et al.*, 2010; Peng *et al.*, 2011), predictions of continued, widespread mortality acceleration (Williams *et al.*, 2013) and declining terrestrial carbon sinks (Arora *et al.*, 2013). Yet, process model predictions of mortality are uncertain because of the complex and interconnected links between vegetation and the hydrologic cycle and the complexity of plant survival mechanisms during droughts (McDowell *et al.*, 2008; McDowell 2011; Anderegg *et al.*, 2012, for reviews).

Two general categories of process models are used to study tree-level drought impacts: (1) detailed models of the soil–plant–atmosphere hydraulic continuum (SPAC) and (2) simpler models simulating only bulk water budgets. The detailed SPAC approach utilizes the cohesion–tension theory to simulate water flux, and detailed numerical hydraulic models of the SPAC have considered a number of factors including: above- and below-ground simulation of water supply, hydraulic properties of the soil and xylem, root distribution and root–shoot ratio (Sperry *et al.*, 1998; Williams *et al.*, 2001; Sperry *et al.*, 2002; McCulloh *et al.*, 2003, 2004; McCulloh & Sperry 2005) and water storage capacitance (Fisher *et al.*, 2006). The drawback of most SPAC models is that they are computationally intensive and require a large number of input parameters, which makes generalization challenging and increases the number of assumptions. The complexity of those models can also render the interpretation and understanding of results difficult, and their calibration is challenging because of the large number of parameters (Blasone *et al.*, 2008; McDowell *et al.*, 2013;

\*Correspondence to: Pierre Gentine, Earth Institutes and Department of Earth and Environmental Engineering, Columbia University, 500 W 120<sup>th</sup> st., Office 842D, New York, NY 10027.  
E-mail: pg2328@columbia.edu

Powell *et al.*, 2013). For instance McDowell *et al.* (2013) performed a comparison of mortality predicted by complex SPAC and land-surface models. The model results agreed that the duration of water stress seemed to be more important than the intensity of the stress per se; yet the interpretation of the controlling factors was hindered by the complexity of the models.

Models that use simplified bulk water budgets have been used effectively to understand hydrological processes and their interconnection during drought but require development to represent more complex processes. For example, Rodríguez-Iturbe I *et al.* (1999), inspired by the earlier work of Eagleson (1978a, b, c, d, e), used soil moisture responses to stochastic rainfall forcing and the role of vegetation structure (mainly rooting depth) to understand the effect of rainfall variability on soil moisture dynamics and vegetation water stress (also see D'Odorico *et al.*, 2000; Porporato *et al.*, 2001). In this reductionist approach, the selected model minimized the number of parameters controlling soil moisture. Vegetation responses to water stress were crudely represented by a linear soil moisture stress function that controls evapotranspiration (*ET*). Application of the model to understand the water stress-induced vegetation mortality requires more complex representation of the physiology and hydraulic control across species and ecosystems (Kumagai & Porporato 2012).

Efforts to bridge the gap between these two modeling approaches have been limited. Schwinning and Ehleringer (2001) provided unique understanding of the role of rooting depth and its interplay with the plant water use, but did not explicitly represent key physiological processes such as embolism, hydraulic capacitance or carbon limitation. Advancing our understanding of drought-induced mortality is likely to require considering the interdependency of carbon starvation (the process of carbohydrate depletion when carbon consumption exceeds carbon gain by photosynthesis) and hydraulic failure (unrepaired loss of hydraulic function leading to subsequent dehydration; McDowell *et al.*, 2011).

The primary objective of this study is to investigate the factors that determine drought resistance using a simplified/hybrid SPAC model. Covariance among tree traits (e.g. biomass, crown area, height and hydraulic conductivity) is constrained through allometric relationships related to tree diameter and wood density, which reduces the number of model parameters because those traits are ultimately interconnected. This simplified SPAC model includes a representation of the soil and plant water budgets. The model is tractable and can capture the essential processes at play while keeping the simplicity required to identify the main processes that underlie drought resistance. The simplicity of the model and interdependence of the traits allows highlighting the main trait controls on drought resistance compared to more sophisticated models which require substantial tuning of parameters.

We evaluate the model with data from a drought experiment in a piñon–juniper woodland in New Mexico (Plaut *et al.*, 2012, 2013; Pangle *et al.*, 2012, Limousin *et al.*, 2013; McDowell *et al.*, 2013). We then explore the parameter space of the model to examine how interspecific variation in tree traits (leaf area index, root:shoot ratio, rooting depth, capacitance and non-structural carbohydrate storage) influences the potential for carbon starvation and hydraulic failure. Finally we investigate the dependence of drought resistance on tree size.

## MODEL DESCRIPTION

The simplified SPAC model is inspired by the model of Farrior *et al.* (2013) but has been expanded to include a refined hydraulic description that can account for cavitation and carbon starvation (Figure 1 and Table I, detailed description in appendix). Below, we give a brief overview of the model components.

### *Tree biomass*

Each tree is composed of its canopy, fine roots and structural biomass. Allometric relationships relate tree height (*Z*), crown area (*W*), structural biomass (*S*), sapwood area, sapwood volume and total leaf area (*L*) to the tree diameter at breast height (*D*), similarly to Farrior *et al.* (2013), as seen in Figure 1. These relationships are constrained using observations of the piñon–juniper dataset (Plaut *et al.*, 2012, 2013; Pangle *et al.*, 2012). Tree leaf area index ( $LAI_{tree}$ ) is the ratio of *L* to *W*. In our model, the trees do not grow because we are investigating the response to a single dry-down period during which we assume no major changes in structural biomass, no leaf or fine-root development and no leaf and root losses. Tree wood density and the related sapwood volume define the maximum stem specific conductivity ( $k_{specific,max}$ ) and maximum stem hydraulic capacitance ( $C_{max}$ ) (Phillips *et al.*, 2004; Scholz *et al.*, 2007). Because we simulate a drought period, we assumed that water is the main limiting resource and nutrient uptake was not constraining.

### *Carbon budget*

Using a simplified Farquhar photosynthesis model (Farquhar & Sharkey 1982; Farquhar *et al.*, 2001) leaves assimilate carbon at a rate proportional to the light level up to their maximum rate of carbon assimilation *V*. Maximum *V* did not vary substantially with water stress for the juniper–piñon dataset used here (Limousin *et al.*, 2013) and is thus assumed to be constant. Light is reduced exponentially at a rate  $k_n$ , as light penetrates into the canopy, following Beer's law. Tree-level photosynthesis is obtained by integration of the leaf-level photosynthesis (Table I—Equation (1)) over the entire canopy (Table I—Equation (2)). Maximum assimilation is

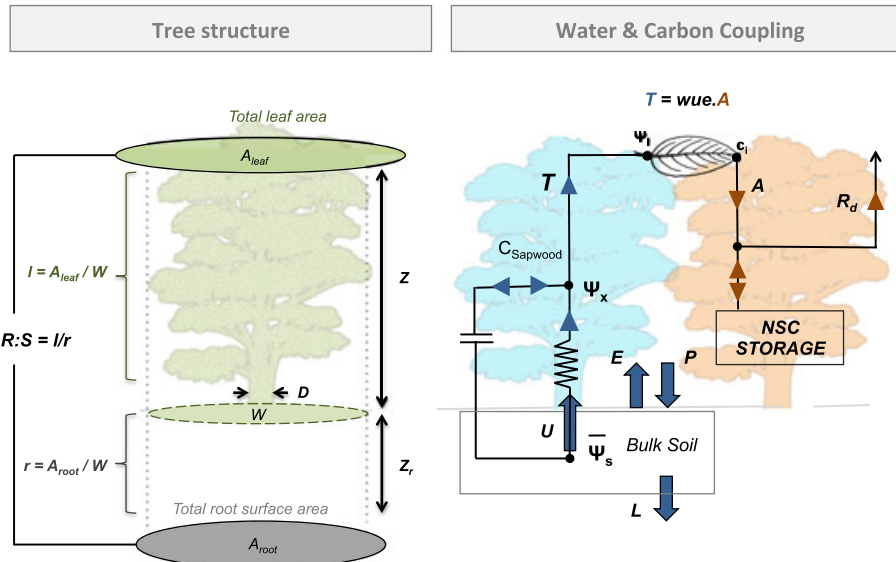


Figure 1. Schematic describing the simplified soil–plant–atmosphere–continuum (SPAC) model introduced in this study.

reduced by a Weibull stress function following (Tuzet *et al.*, 2003) (Table I—Equation (3)), which depends on xylem water potential  $\psi_x$  (Zhang *et al.*, 2012). This Weibull stress function can represent a range of stomatal behaviours from relatively isohydric to more anisohydric (Meinzer & McCulloh 2013). Relatively anisohydric species (juniper in this study) exhibit a pronounced change in leaf-water potential with evaporative demand and depletion of soil moisture via maintenance of stomatal conductance. On the other hand more isohydric species maintain a relatively constant mid-day minimum leaf-water potential through strong reduction in stomatal conductance (Tardieu and Simonneau 1998, Schultz 2003; Plaut *et al.*, 2012).

Here we focus on variations in non-structural carbon (NSC) during a drought, during which growth is assumed to be negligible. Growth decreases faster than photosynthesis in response to drought in most vascular plants (McDowell *et al.*, 2011, 2013). NSC then drops when photosynthesis is reduced by water stress and becomes insufficient to compensate respiration. Here we consider a single dry-down event and assume that the initial NSC is a fraction  $\alpha_{NSC}$  of the root and canopy dry biomass (Sevanto *et al.*, 2013). NSC is lost through maintenance respiration  $R$  of fine roots  $R_r$ , sapwood  $R_{sw}$  and leaves  $R_l$  (Farrior *et al.*, 2013). We assume a mean respiration rate during the drought period rather than incorporate variation in respiration rate within and between days (based on Mahecha *et al.*, 2010).

### Water budget

The prognostic equation for soil moisture is based on a simple bucket water budget over a volume with depth  $z_r$ , the effective rooting depth (Eagleson 1978c), and which extends over an area  $rW$  (Table I—Equation (5)), with  $W$  the crown area and

the relative area coverage of roots versus crown (Appendix S11). The source of soil moisture is precipitation  $P$ , and the sinks are a leakage term comprising runoff and infiltration to deeper soil layer  $L$ , bare soil evaporation  $E$  and root water uptake  $U$  per unit crown area.  $U$  is related to the water potential difference between the xylem  $\psi_x$  and soil  $\psi_s$  following Darcy's law and is proportional to the fraction of root per unit crown area  $r$  (Table I—Equation (6)) (Sperry *et al.*, 1998). Bare soil evaporation is related to above canopy potential evaporation  $E_p$ , attenuated by shading according to Beer's law and limited by a soil moisture stress function dependent on soil water potential (Table I—Equations (7) and 7) (Albertson & Montaldo 2003; Gentine *et al.*, 2012). During a dry-down there is neither precipitation nor infiltration so that the only processes affecting soil moisture are bare soil evaporation and root water uptake.

Transpiration is related to tree-level photosynthesis through intrinsic water-use efficiency ( $wue$ ) (Table I—Equation 8). The volumetric water content ( $VWC$ ) of the tree is increased by the total base flow (root water uptake)  $WU$  and reduced by transpiration  $WT$  (Table I—Equation (9)) (Tuzet *et al.*, 2003). Changes in  $VWC$  are related to xylem water potential changes through the capacitance  $C_w$ , which depends on the xylem water potential itself and wood density of each species (Table I—Equation 10). Inclusion of capacitance may be important in some species because it affects the hydraulic safety margins for many species (Meinzer *et al.*, 2008, 2009).

Because the model is largely described by allometric relationships the main input of the models are reduced to: (i) wood dry density  $r_d$ , (ii) diameter at breast height (130-cm height; DBH), (iii) rooting depth  $z_r$  and root:shoot ratio, (iv) the parameters of the simplified Farquhar photosynthesis model ( $V$  and the quantum efficiency) and (v) the  $wue$ . Root:

Table I. List of variables with units and notation/equation.

Variable	Units	Notation/equation	Equation number	Source
<i>Universal constants</i>				
Gravity	$\text{m s}^{-2}$	$g$		
Water density	$\text{kg m}^{-3}$	$\rho_w$		
<i>Plant parameters</i>				
Tree structure				
Stem diameter	cm	$D$		
Height	m	$Z = HD^{\gamma-1}$		
Crown area	$\text{m}^2$	$W = a_w D^{\gamma} W$		
Crown diameter	m	$D_c = 2(W/\pi)^{1/2}$		
Wood density	$\text{g cm}^{-3}$	$r_d$		
Rooting depth	m	$z_r$		
Total leaf area	$\text{m}^2 \text{ m}^{-2}$	$A_{leaf} = a_l D^{b_l}$		
Leaf area index	$\text{m}^2 \text{ kg}^{-1}$	$l = A_{leaf}/W$		
Specific leaf area	$\text{m}^2 \text{ m}^{-2}$	$SLA$		
Root area index		$r$		<i>dataset</i>
<i>Hydraulic</i>				
Sapwood area	$\text{m}^2$	$A_{SW} = a_{SW} D^{b_{SW}}$		Meinzer <i>et al.</i> (2005)
Sapwood volume	$\text{m}^3$	$V_{SW} = A_{SW} Z$		
Leaf specific conductivity (roots to leaves)	$\text{kg m}^{-1} \text{ s}^{-1} \text{ MPa}^{-1}$	$k_{leaf \text{ specific}} = k_{leaf \text{ specific,max}}(1 - PLC)$		
Maximum leaf specific conductivity (roots to leaves)	$\text{kg m}^{-1} \text{ s}^{-1} \text{ MPa}^{-1}$	$k_{leaf \text{ specific,max}} = k_{leaf \text{ specific,max}} S/A_{leaf}$		
Maximum specific conductivity (roots to leaves)	$\text{kg m}^{-1} \text{ s}^{-1} \text{ MPa}^{-1}$	$k_{S \text{ specific,max}} = 0.22 + 9.22 \exp(-6.1 r_d)$		Bucci <i>et al.</i> , (2004)
Percent loss of conductivity	%	$PLC = 100(1 - \exp(-(\psi_x/\psi_k)^{c_k}))$		Bucci <i>et al.</i> (2004)
Percent loss of conductivity	%	Linearized: $PLC = \min\left(\max\left(100\left(1 - \frac{\psi_x - \psi_{x,\min}}{\psi_x - \psi_{x,\min}}\right), 0\right), 1\right)$		Plaut <i>et al.</i> (2012)
Root-xylem conductance (per unit surface crown)	$\text{kg m}^{-2} \text{ s}^{-1} \text{ Pa}^{-1}$	$g_{root-xylem} = k_{leaf \text{ specific}}/Z$		
Stomata and hydraulic conductivity stress function (linearized)	—	$f(\psi_x) = \min\left(\max\left(\frac{\psi_x - \psi_{x,\min}}{\psi_{x,\min} - \psi_{x,\min}}, 0\right), 1\right)$		
Max sapwood capacitance	$\text{kg m}^{-3} \text{ MPa}^{-1}$	$C_{w,max} = \max(416-619 r_d, 10)$		Scholz <i>et al.</i> (2007)
Tree max sapwood capacitance	$\text{kg MPa}^{-1}$	$C_{w,max} = C_{w,max} \times V_{SW}$		Scholz <i>et al.</i> (2007)
Tree capacitance	$\text{kg MPa}^{-1}$	$C_w = C_{w,max} \exp\left(-\left(\frac{\psi_x}{\psi_c}\right)^{c_k+1}\right)$	(10)	Edward <i>et al.</i> , (1982)
<i>Carbon assimilation</i>				
Extinction coefficient	—	$k_p = 0.4$		Beer's law
Light level below $l$ leaf layers	$\text{W PAR m}^2$	$L = L_0 \exp(-k_p l)$		Beer's law
Carbon fixation/light intensity	$\text{kg CO}_2 \text{ J PAR}^{-1}$	$a_f$		CLM
Leaf-level carbon assimilation (non-water limited)	$\text{kg CO}_2 \text{ m}^{-2} \text{ s}^{-1}$	$A_x = \min(a_f L, V)$	(1)	Farrion <i>et al.</i> (2013)

Tree-level carbon assimilation (non-water limited)	$\text{kgCO}_2 \text{ m}^{-2} \text{ s}^{-1}$	$A_t = \min(a_f L_0(1 - \exp(-k_r D), VI)$	(2)	Farrion <i>et al.</i> (2013)
Tree-level carbon assimilation (water limited)	$\text{kgCO}_2 \text{ m}^{-2} \text{ s}^{-1}$	$A = A_t f(\psi_x)$	(3)	Farrion <i>et al.</i> (2013)
Carbon respiration				
Fine-root respiration per unit root area	$\text{kgCO}_2 \text{ m}^{-2} \text{ s}^{-1}$	$R_r$		
Fine-root respiration	$\text{kgCO}_2 \text{ s}^{-1}$	$R_r = p_r r W$		
Leaf respiration per unit area	$\text{kgCO}_2 \text{ m}^{-2} \text{ s}^{-1}$	$p_l$		
Leaf respiration per tree	$\text{kgCO}_2 \text{ s}^{-1}$	$R_l = p_l l W$		
Sapwood respiration per unit sap volume	$\text{kgCO}_2 \text{ m}^{-3} \text{ s}^{-1}$	$R_{sw}$		
Sapwood respiration	$\text{kgCO}_2 \text{ s}^{-1}$	$R_{sw} = p_{sw} V_{sw}$		
Water budgets				
Soil water budget	$\text{kg m}^{-2} \text{ s}^{-1}$	$\rho_w z_r n \frac{d\psi}{dt} = P - U - E - L$	(4)	
Tree water budget	$\text{kg s}^{-1}$	$C_{w, \max} \frac{dV}{dt} = W(U - T)$	(9)	
Carbon budgets				
Non-structural carbon budget	$\text{kg m}^{-2} \text{ s}^{-1}$	$\frac{dNSC}{dt} = A - R_d$		
Soil hydrology				
Potential evaporation	$\text{kg m}^{-2} \text{ s}^{-1}$	$E_p$		Penman-Monteith
Soil evaporation	$\text{kg m}^{-2} \text{ s}^{-1}$	$E_s = E_p (1 - \exp(-k_r l)) f_s(\psi_s)$	(6)	Gentile <i>et al.</i> (2012)
Soil evaporation water stress function	—	$f_s(\psi_s) = \min\left(\max\left(\frac{\psi_s - \psi_h}{\psi_c - \psi_h}, 0\right), 1\right)$	(7)	Dai <i>et al.</i> , (2003)
Water-use efficiency	$\text{kgCO}_2 \text{ kgH}_2\text{O}$	$wue$		
Transpiration	$\text{kgH}_2\text{O m}^{-2} \text{ s}^{-1}$	$T = A / wue$	(8)	
Basal sap flow	$\text{kg m}^{-2} \text{ s}^{-1}$	$U = r g_{root} - xylem(\psi_s - \psi_x - \rho_w g Z) = G_{total} \Delta\psi$	(6)	
Soil water potential	Pa	$\psi_s$		Brooks and Corey (1964); Eagelson (1978)
Potential at saturation	Pa	$\psi_{sat}$		Brooks and Corey (1964)
Relative soil moisture	—	$s = (\psi_s / \psi_{sat})^{1/b}$		
Shape parameter of Brooks & Corey curve	—	$b$		
Pore disconnectedness index	—	$m = 2b + 3$		Brooks and Corey (1964)
Infiltration term	$\text{kg m}^{-2} \text{ s}^{-1}$	$L = \rho_w K_{sat} s^m$		Brooks and Corey (1964)
Saturated water content	$\text{m}^3 \text{ m}^{-3}$	$n$		Brooks and Corey (1964)

shoot area ratio is assumed to be 1 for piñon and 0.3 for juniper following West *et al.* (2008), but a sensitivity test will be performed later in the manuscript. The remaining model parameters ( $z_r$ ,  $V$ ,  $\alpha_f$ ) are calibrated so that the model best fits the observations (see below). Fitted parameter values are given in Table I.

#### *Hydraulic failure—carbon starvation*

**Hydraulic failure.** The hydraulic failure hypothesis predicts that substantial and irreversible embolism leads to mortality. The rhizosphere and xylem cavitate (i.e. fill with air) as a function of decreasing water potential leading to a progressive reduction in the liquid water soil–plant continuum (Tyree & Sperry 1989; Sperry *et al.*, 2002). If embolism persists and expands the plant may desiccate and die. In the model, hydraulic failure is defined when the percentage loss in conductivity (PLC) in the xylem reaches 98%, which defines the corresponding critical xylem potential  $\psi_{crit}$ . This 98% threshold is arbitrary but corresponds to an important loss of conductivity and therefore to loss of resistance to biotic agents and external disturbances. In addition the choice of the threshold does not modify the general conclusions made in the manuscript and only delays the time to desiccation.

**Carbon starvation.** In the model, carbon starvation is defined as the time when NSC reaches 2% of dry mass (in parallel with the 98% threshold used for the PLC); in the *in situ* observations almost none of the trees went below this threshold (McDowell *et al.*, 2013). In reality NSC may also be used to refill the embolized conduits (Secchi & Zwieniecki 2011) and the drought may limit phloem transport of carbohydrates to sites where they are needed (Sevanto *et al.*, 2013) such that the actual carbon starvation process is intimately coupled to plant desiccation (McDowell *et al.*, 2011). The use of this NSC threshold provides insight into the processes affecting NSC resources. The definition of carbon starvation could easily be made more complex in future model versions. Our objective here is to focus on the role of plant traits on the tendency of carbon starvation and hydraulic failure rather than on the exact date of death, which may also depend on other factors (e.g. biotic attacks, McDowell *et al.*, 2013).

#### *Dry-down: Stage 1–Stage 2 transpiration/photosynthesis*

To assess the effect of different traits and parameters on hydraulic failure and carbon starvation, the model is solved for a dry-down where precipitation, runoff and infiltration do not occur. Growth is then assumed to be negligible during this dry-down, and the focus is on the NSC budget. Two initial conditions are required: the initial soil water potential  $\psi_{s,0}$ , chosen as the field capacity  $-0.33$  MPa, and the initial NSC, prescribed as a fraction of the sum of the leaf

and root biomass,  $\alpha_{NSC}^0$ , which depends on the history preceding the dry-down. We chose a nominal initial NSC content of 10% (McDowell *et al.*, 2013) for both species. Wetter antecedent conditions would result in higher  $\psi_{s,0}$  and different  $\alpha_{NSC}^0$  (McDowell *et al.*, 2011). We then integrate the water and carbon budget equations (see appendix and table) to determine: (i) the time spent in a regime with negligible embolism (stage 1 regime see below)  $\tau_1$  until the xylem potential reaches  $\psi_e$ , (ii) the time spent in the embolized regime until hydraulic failure (stage 2 regime see below)  $\tau_2$  when the xylem potential reaches its critical value  $\psi_{crit}$  and (iii) the time required to deplete the NSC reserves  $\tau_{starvation}$ .

Drawing upon the literature on bare-soil evaporation (Salvucci 1997), which defines stage-one (energy-atmospheric demand limited) and stage-two (soil moisture limited) phases of soil dry-down, we introduce the concept of stage-one and stage-two transpiration and photosynthesis. During stage one, embolism is negligible, and gas exchange is mostly limited by evaporative demand and photosynthetically active radiation (PAR). During stage one, photosynthesis is high, and NSC reserves are increasing, providing further resistance to carbon starvation. Anisohydric traits favour time spent within this energy-limited regime because stomata remain open (McDowell *et al.*, 2011; Meinzer & McCulloh 2013), as shown in Figure 2. A delay in the onset of embolism corresponds to a longer stage 1.

During stage 2, transpiration and photosynthesis are reduced below their maximum rates by embolism in the soil to stomata pathway and are therefore water limited (Table I—Equation (3)). If respiration exceeds photosynthesis, while growth is zero, NSC decreases (McDowell *et al.*, 2011). Some plants display isohydrodynamic behaviour (Franks *et al.*, 2007), in which the soil to leaf water potential gradient is relatively constant. More isohydric species tend to spend more time within the stage 2, during which they reduce leaf-gas exchange through stronger stomata regulation, and as a consequence are more prone to carbon starvation than anisohydric species (Meinzer & McCulloh 2013). The variety of plant behaviour is represented through changes in the Weibull-curve control of stomatal opening and closure and embolism as depicted in Figure 2 (Meinzer & McCulloh 2013, Table I—Equation (3)). A longer stage 2 refers to a delayed time to full hydraulic failure from the onset of embolism. Figure 3 depicts an example of times series of gross primary productivity generated by the model and corresponding soil moisture and highlights the stage 1 (not water stressed) and stage 2 (water stressed) periods.

## DATASET

### *Site description*

The dataset is described in detail in Pangle *et al.* (2012) and Plaut *et al.* (2012). The study was conducted in the Los

SURVIVAL STRATEGIES OF HYDRAULIC FAILURE AND CARBON STARVATION

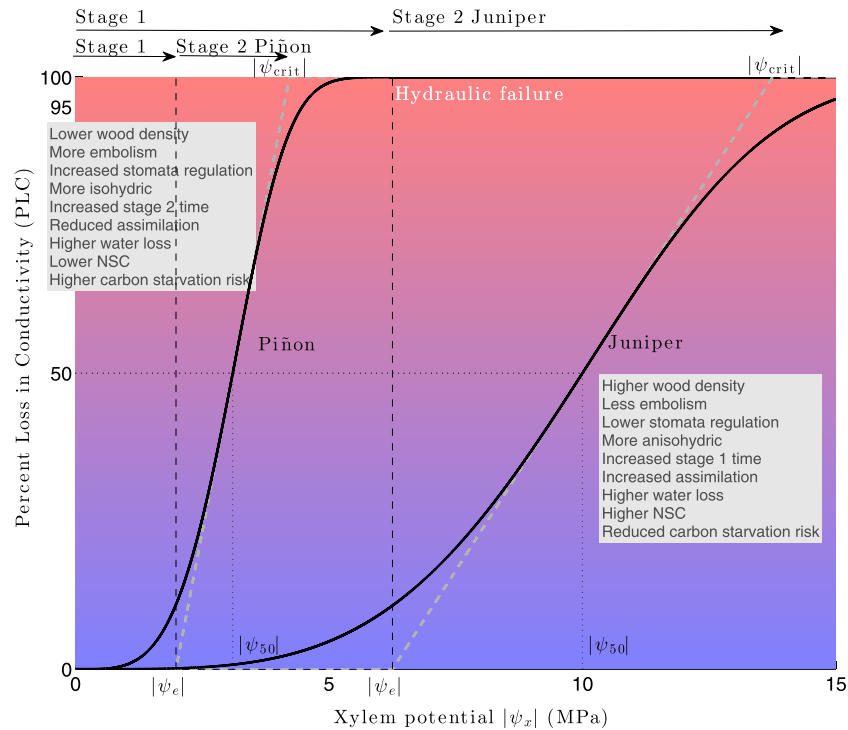


Figure 2. Schematic describing the effect of the vulnerability curve on hydraulic failure and stage 1 (no embolism) and stage 2 (embolized) regimes up to hydraulic failure define when the xylem potential reaches  $\psi_{crit}$  after Meinzer and McCulloh (2013).

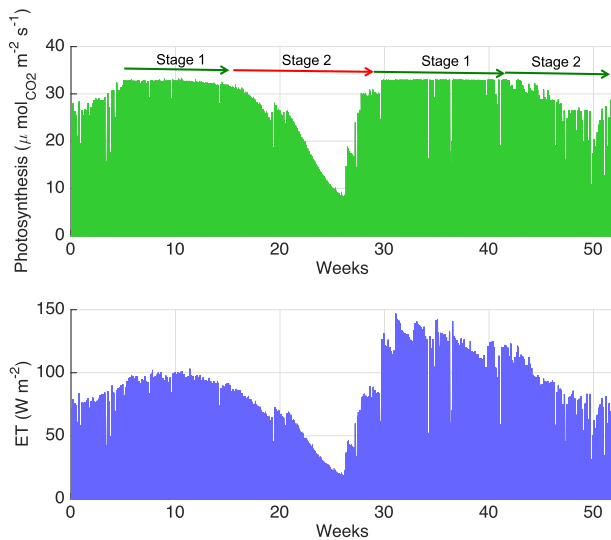


Figure 3. (top) Time series of simulated tree gross primary productivity generated by the model, and corresponding phase 1 (unstressed) and phase 2 (stressed) periods as well as total evapotranspiration (transpiration plus bare soil evaporation) (bottom).

Piños mountains within the Sevilleta National Wildlife Refuge, Socorro County, New Mexico (N 34°23'13", W 106°31'29", elevation 1911 m), part of the US Long-Term Ecological Research network. Piñon pine (*Pinus edulis*) and one-seed juniper (*Juniperus monosperma*) are the dominant woody species. Soils are calcid aridisols characterized as

Sedillo–Clovis association of fan alluvium derived from conglomerate. Long-term mean monthly temperatures range from 2.6 °C in January to 23.1 °C in July; annual precipitation averages 362 mm. Roughly half of the annual precipitation falls can be attributed to convective storms during the North American Monsoon, from July to September.

The data were obtained from a precipitation manipulation experiment at the site which includes three levels of water: control, irrigated and drought (Pangle *et al.*, 2012). Here, we only consider the ambient control blocks, which are composed of three blocks (flat, south-facing slope and north-facing slope). Treatments began in the summer of 2007. Full details of the experiment and plots are provided in Pangle *et al.* (2012) and Plaut *et al.* (2012).

*Tree data*

Within each of the three plots, five trees of each species were chosen for physiological measurements including sap flux density, leaf water potential and soil moisture (Pangle *et al.*, 2012). These target trees were centrally located within the plots and had stem(s) of at least 9-cm diameter. The plots included over 50 piñon trees with average DBH of 21.54 cm with variations from 5 to 40 cm and over 65 junipers with mean DBH of 31 cm with variations from 5 to 75 cm.

*Plant water potential*

Pre-dawn and midday leaf water potentials ( $\psi_{pd}$  and  $\psi_{md}$ , respectively) were measured on each target tree using

south-facing twigs with healthy foliage. Measurements were made 5–10 times a year, when soil moisture was changing rapidly during each summer's dry-down and monsoon. We used leaf and soil water potential measurements to constrain the dynamics of the simplified SPAC model to achieve both realistic soil moisture and leaf water potential temporal dynamics (see Model results section).

#### Cavitation vulnerability

Curves describing xylem vulnerability to drought-induced cavitation (Sperry *et al.*, 1988) were generated using the centrifuge technique (Cochard 2002; Cochard *et al.*, 2005). Percent loss of conductance (PLC) was plotted against pressure and fit to a Weibull function to generate a vulnerability curve (Neufeld *et al.*, 1992). Xylem vulnerability was measured on piñon and juniper branches. The Weibull function parameters for piñon were on average  $\psi_{50} = -3.4$  MPa (xylem point of 50% drop in PLC) and  $c_k = 4$  (shape of the retention curve), and for junipers  $\psi_{50} = -11$  MPa and  $c_k = 3.85$ . Those values are imposed in the simplified SPAC model.

#### Moisture data

A micrometeorological station at the research site included a Campbell Scientific HMP45C air temperature and relative humidity sensor (Logan, UT, USA), tipping bucket rain gauge equipped (Pockman & McDowell 2006), Decagon EC-20 soil volumetric water sensor installed at 5 cm (Decagon Devices Inc., Pullman, WA, USA—Pockman & McDowell 2013) and net radiometer (model NR-LITE, Kipp & Zonen, Delft, The Netherlands). Plant-available soil moisture was measured with thermocouple psychrometers (Wescor Inc., Logan, UT, USA—Pockman & McDowell 2014) and recorded with Campbell Scientific CR-7 dataloggers.

## MODEL RESULTS

#### Comparison with observations

The model correctly captures the seasonal cycle and different dry downs of the soil potentials. Figure 4 depicts the modeled soil water potential against observations in the deep soil layers located within 50 to 100 cm for both piñons and junipers. The model response is buffered compared to the deepest soil water potential measurement ((1) m) because piñon and juniper typical rooting depths are much deeper than the deepest measurement ((1) m), introducing important temporal buffer on soil moisture and water potential temporal dynamics (Gentine *et al.*, 2012). The seasonal dynamics and range of the leaf water potential at predawn  $\psi_{pd}$  is reasonably reproduced for both species as seen in Figure 5 ( $R^2 = 0.85$  for junipers and  $R^2 = 0.55$  for piñons).

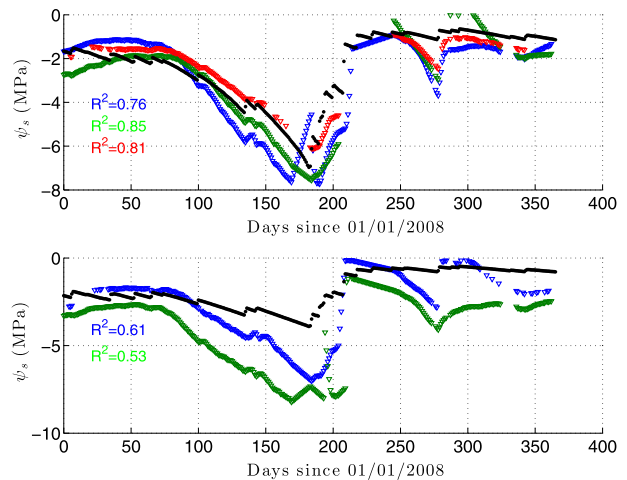


Figure 4. Time series of modeled (black) deep soil water potential compared to observations located between 50 to 100 cm (coloured diamonds) over five of the ambient control experiment plots for junipers (top) and piñons (bottom). Measurements are limited to 100 cm which is shorter than typical rooting depth, hence the damped signal in the model output.

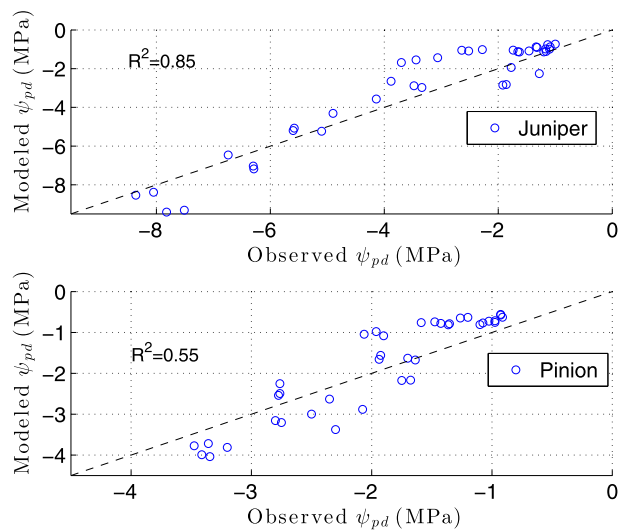


Figure 5. Modeled versus observations of leaf water potential at predawn (subscript pd) for junipers (left) and piñons (right).

These results emphasize that the simplified SPAC model realistically captures the seasonal course of soil and leaf water potential. A summary of the model parameters is presented in Tables II and III.

#### Root:shoot ratio

We first investigate the role of tree leaf area index (tree LAI) and root:shoot ratio (R:S) on hydraulic failure and carbon starvation, while other factors (Table I) were held constant. For all but very low LAI, increasing piñon R:S extended the length of stage 1, when water stress is minimal, but decreased the time to the end of stage 2, when water stress is prevalent (Figure 5). As a result of these

offsetting effects, the number of days to hydraulic failure is relatively insensitive to the R:S ratio across a range of LAI. On the other hand higher R:S strongly decreased the days to carbon starvation because higher partitioning of the biomass into the shoot is beneficial for increased carbon assimilation. An optimal tree LAI exists of the order of  $2\text{ m}^2\text{ m}^{-2}$ —as typically observed for *P. edulis*—to avoid hydraulic failure (Figure 5c). In the model, lower tree LAI is detrimental because it is associated with higher bare soil evaporation and therefore earlier soil drying. Higher LAI also reduces the time to hydraulic failure because it results in water overuse by tree transpiration. Increased tree LAI reduces the number of days to carbon starvation because higher tree photosynthesis cannot compensate for higher tree water usage and maintenance costs, further emphasizing the tight coupling between the water and carbon cycles for carbon starvation. With our model the time to starvation is always longer than the time to hydraulic failure (at least 1.3 times more—results not shown).

The model indicated that the time juniper spent in stage 1 and 2 was also not very sensitive to changes in R:S (Figure 6) but was highly dependent on the tree LAI. The optimal LAI based on the duration of stage 1 was  $1.3\text{--}2.0\text{ m}^2\text{ m}^{-2}$ , a result that is consistent with field measurements of juniper LAI ( $1.5\text{--}2.0$  in West *et al.*, 2008). As for piñon, juniper time to carbon starvation strongly decreases with increased tree LAI and R:S ratios.

For junipers (Figure 7) the time to carbon starvation is generally longer than the time to hydraulic failure (ratio ranging from 1.1 to 2.4) unless trees have very low tree LAI (less than  $1\text{ m}^2\text{ m}^{-2}$ ) or high R:S (not shown). In general the time to carbon starvation is 50 to 100% larger than the time to hydraulic failure for large LAI ( $>1\text{ m}^2\text{ m}^{-2}$ ) and low R:S ( $<2$ ).

#### Anisohydric–isohydric behaviour—loss of conductivity

We now turn to the role of the vulnerability curve on hydraulic failure and starvation. Stomatal control of transpiration-induced xylem tension is an important mechanism for avoiding excessive embolism. The shape of the vulnerability curve is representative of a range of behaviours from anisohydric to isohydric (Figure 2 and Meinzer & McCulloh 2013). Isohydric and anisohydric behaviours represent two extremes of a continuum of regulation of xylem tension (Meinzer & McCulloh 2013). We thus study the effect of the xylem vulnerability curves and stomatal regulation on the survival to hydraulic failure and carbon starvation as a way to represent different regulation mechanism from anisohydric to isohydric.

The parameter  $|\psi_{50}|$  represents the inflection point—50% loss of conductivity—in absolute value and  $c_k$  is the slope of the PLC at  $|\psi_{50}|$ , i.e. the sharpness of the cavitation curve. Similar water stress response is assumed for

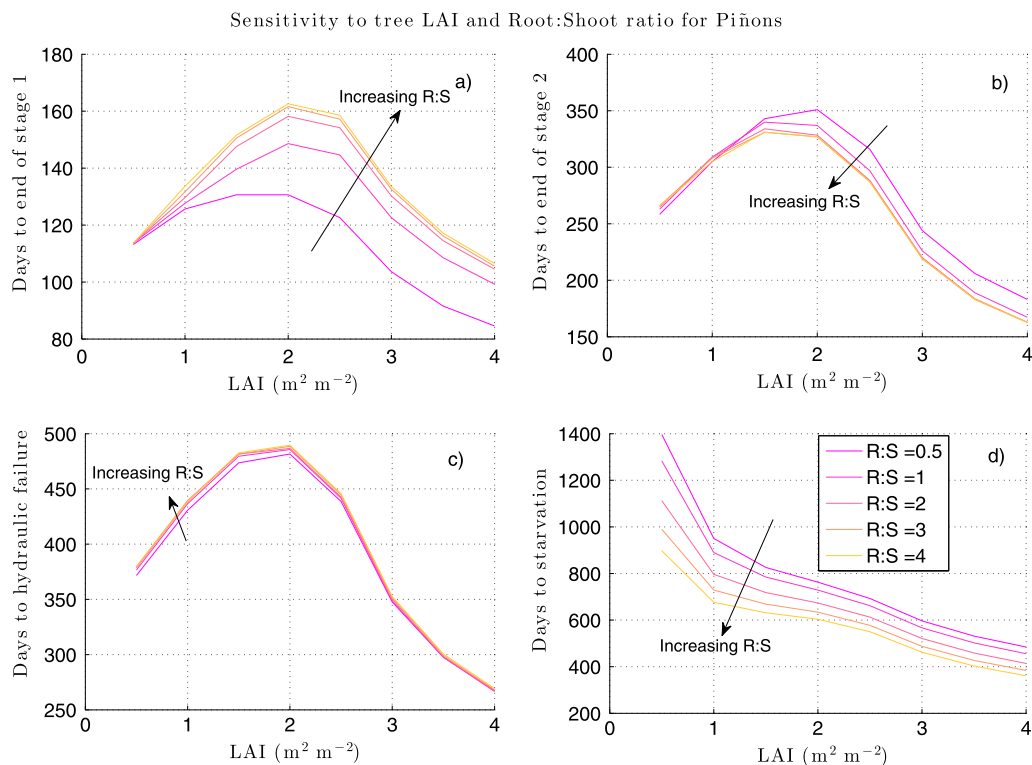


Figure 6. Sensitivity of number of days spent in stage 1 (top left), in stage 2 (top right), to hydraulic failure (bottom left) and time to carbon starvation to tree leaf area index (tree LAI) and root:shoot area for piñons.

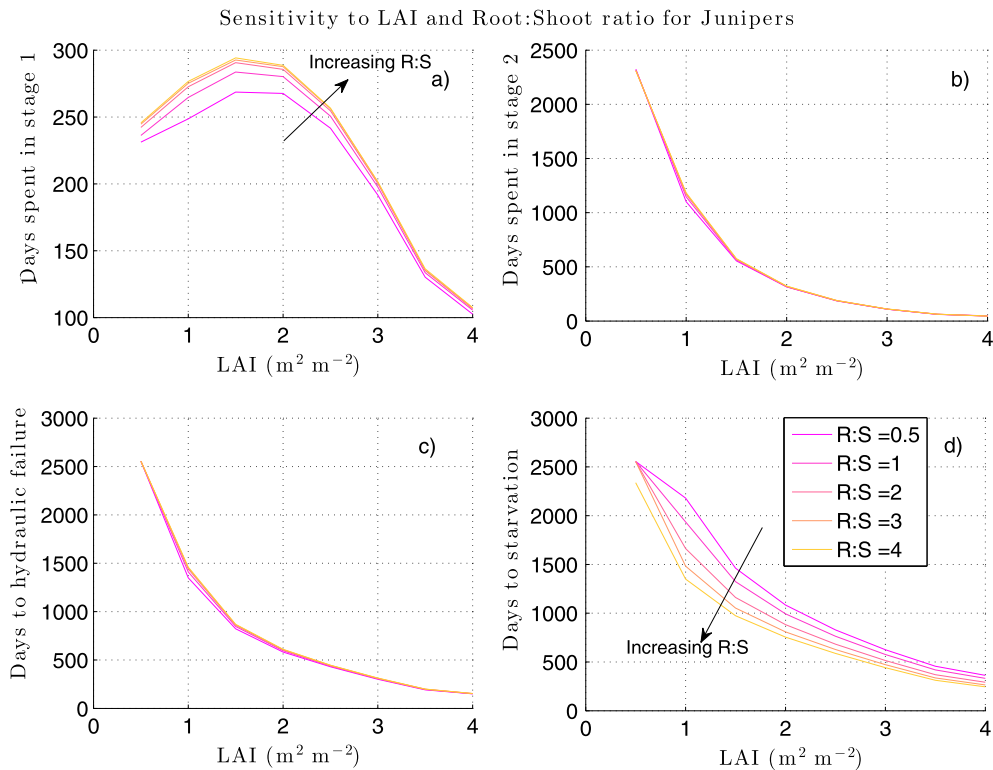


Figure 7. Same as Figure 6 but for junipers.

stomatal regulation (Equation (3)) (Manzoni *et al.*, 2013). When  $|\psi_{50}|$  is low, embolism is minimal, and the behaviour is closer to anisohydric. The higher  $c_k$ , the sharper the transition from stage 1 to stage 2. Higher  $|\psi_{50}|$  increases the duration of stage 1 for both piñons (Figure 8) and junipers (Figure 9) as could be expected because the onset of embolism is shifted to a more stressed regime (higher  $\psi_x$ ). The stage 1 regime of junipers is more sensitive to variations in  $|\psi_{50}|$  than that of piñons. Indeed piñons are more frequently in a stressed (stage 2) regime, with stomatal regulation induced by water stress, and are thus more sensitive to stage 2. Higher  $|\psi_{50}|$  increases the duration of stage 2 for both piñons (Figure 8b) and junipers (Figure 9b). However at high  $|\psi_{50}|$  the number of days spent in stage 2 saturates. There is thus little added benefit in having a cavitation curve with high absolute  $|\psi_{50}|$ , i.e. narrow tracheid diameter (Brooks & Corey 1964; Brutsaert 2005). The time to hydraulic failure (combined stage 1 and stage 2) increases with  $|\psi_{50}|$ , yet at high  $|\psi_{50}|$  the time to hydraulic failure flattens, and there is only marginal benefit in having further  $|\psi_{50}|$  increase. Very similar patterns are observed for the time to carbon starvation.

The sharpness of the cavitation curve,  $c_k$ , increases the duration of stage 1 for both piñons and junipers: sharper cavitation curves delay the onset of embolism (in terms of xylem potential). Consequently, a sharper cavitation curve reduces the time spent in stage 2 for both species (Figure 8b).

Overall the time to hydraulic failure is very sensitive to the sharpness of the cavitation curve,  $c_k$  (Figure 8c and Figure 9c). Higher  $c_k$  decreases the time to hydraulic failure: the increased stage 1 duration cannot compensate the substantial stage 2 decrease for both piñons and junipers. Stage 2 (embolized) regime is thus the dominant control on the time to hydraulic failure. Similar conclusions are reached for the time to carbon starvation for both species, higher  $c_k$  decrease the time to carbon starvation. Stage 2 is the dominant mechanism here and corresponds to a regime of partial stomatal closing under water stress and therefore reduced photosynthesis, which impact the NSC pool.

Smoother cavitation curve and higher  $|\psi_{50}|$  increase the resistance to hydraulic failure and to carbon starvation, as seen in Figure 8 and Figure 9. In dry cases, i.e. at high  $|\psi_{50}|$  (>6–8 MPa), there is only marginal increase in drought resistance with increasing  $|\psi_{50}|$ ; it is then more beneficial to reduce the sharpness of the retention curve  $c_k$ . The sharpness of the retention curve is related to the distribution of tracheid diameters (Brooks & Corey 1964; Brutsaert 2005). Higher  $c_k$  represents a wider relative distribution of tracheid diameters. It is thus beneficial for the xylem to have a narrow distribution of tracheid diameters, which reduces  $c_k$ , and the risk of hydraulic failure and carbon starvation for a given  $|\psi_{50}|$ . The combination of higher  $|\psi_{50}|$  and  $c_k$ , which corresponds to narrower tracheid diameter and narrower distribution of diameters, respectively,

SURVIVAL STRATEGIES OF HYDRAULIC FAILURE AND CARBON STARVATION

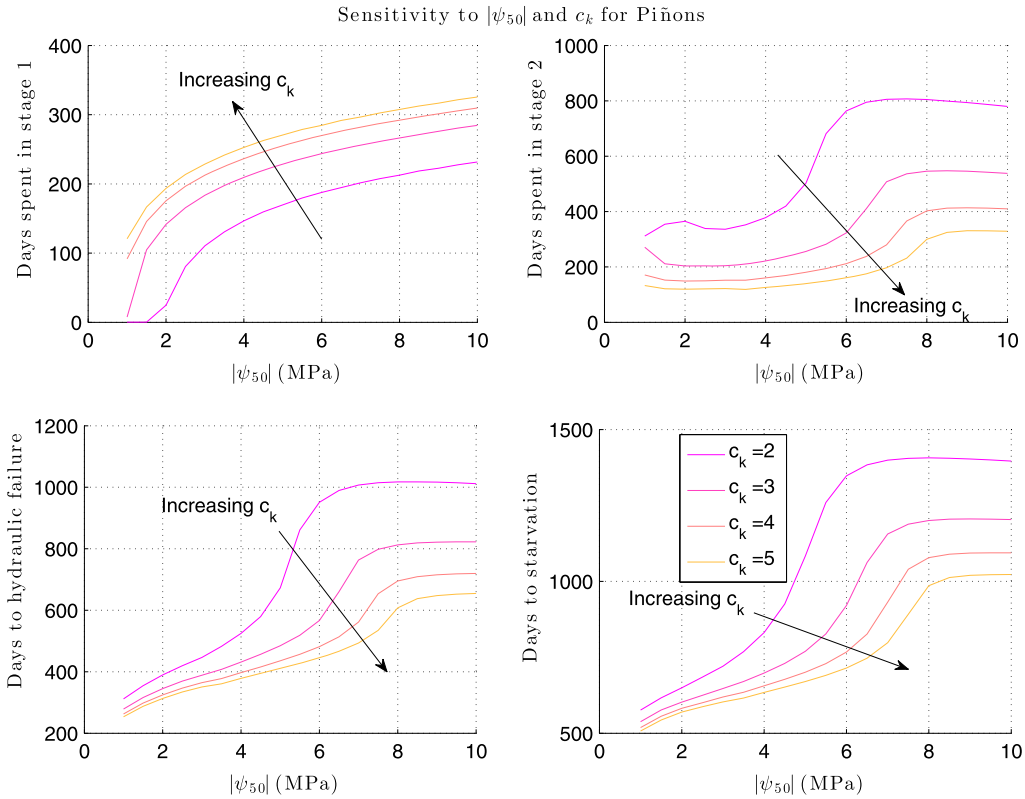


Figure 8. Sensitivity of the number of days spent in stage 1 (top left), in stage 2 (top right), time to hydraulic failure (sum of stage 1 and stage 2—bottom left) and time to carbon starvation (bottom right) to the parameters of the vulnerability curve  $\psi_{50}$  (point of 50% loss of conductivity) and  $c_k$  shape parameter of the cavitation curve for piñons.

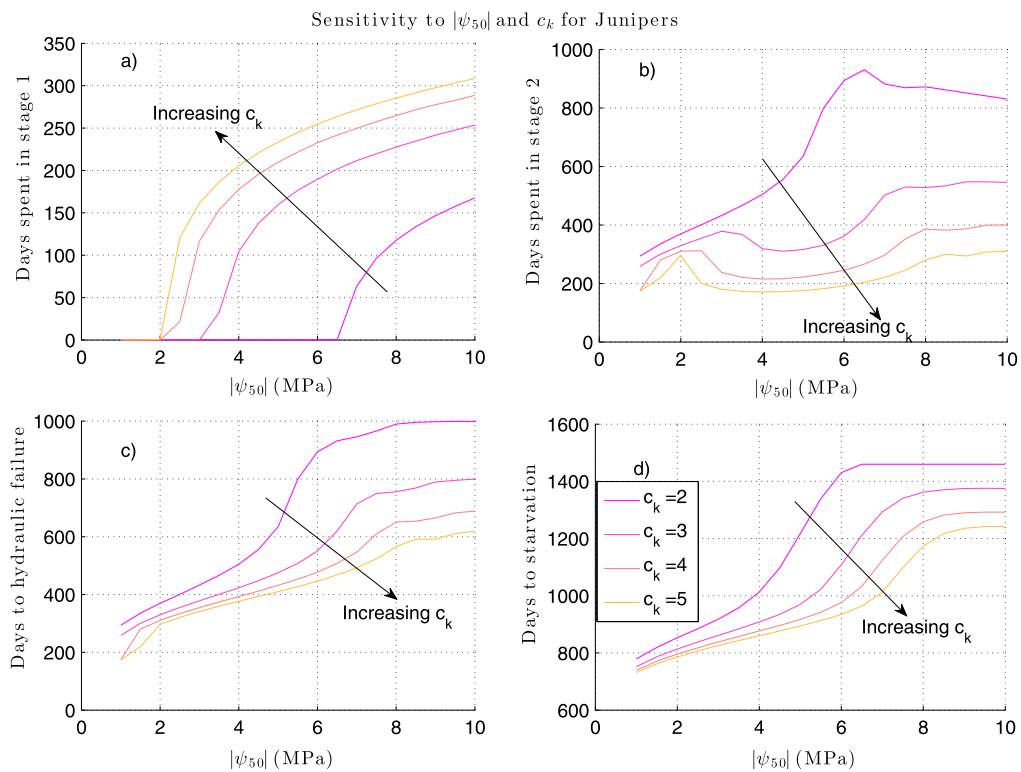


Figure 9. Same as Figure 7 but for junipers.

reduces the risk of hydraulic failure and carbon starvation, in line with observations of juniper and piñon resistance to drought (Linton *et al.*, 1998).

To assess the consequences of the specific effect of different cavitation curves and anisohydric versus isohydric stomatal regulation compared to other traits we simulated a piñon with cavitation curve characteristic and stomatal water-stress response similar to those of juniper; that is we simulate an ‘anisohydric’ piñon. All other model parameters such as root:shoot ratio, maximum hydraulic conductivity and tree LAI were kept identical to their reference values (Table I). With the increased protection against embolism onset the ‘anisohydric’ piñons increase their time to hydraulic failure from 352 to 768 days and increase the time to carbon starvation from 637 to 846 days. Interestingly, compared to junipers, the ‘anisohydric’ piñons are slightly more resistant to hydraulic failure (768 days for ‘anisohydric’ piñons vs. 736 days for junipers), even with their higher LAI. Based on the model sensitivity analysis, the higher maximum—non-embolized—tree hydraulic conductance of piñons is the main explanation for this difference. Higher maximum conductivity reduces the drop of water potential in the leaves and in the xylem, and thus reduces the impact of soil moisture depletion on the xylem cavitation and stomatal closure. The opposite effect is seen on carbon starvation, which is achieved much later at 1056 days for junipers compared to 846 days for piñons because of stomatal closure and higher respiration maintenance rates of piñons. The main factor explaining the increased survival resistance of juniper compared to the ‘anisohydric’ piñons is its lower leaf area index. This analysis confirms that it is not a single trait, in this case the shape of the vulnerability curve, but rather the set of all traits that determine the drought resistance of different species.

#### *Anisohydric–isohydric behaviour—theoretical analysis*

In the case of negligible capacitance, the minimum midday xylem water potential  $\psi_{x,\text{midday}}$  can simply be related to the soil water potential  $\psi_s' = \psi_s - \rho g Z$ :

$$\psi_{x,\text{md}} = \psi_s' - \Delta\psi, \quad (1)$$

with  $\Delta\psi$  the diurnal drop of xylem water potential and  $A_L^{\text{md}}$  the peak daily photosynthetic flux, regulated by stomatal control (Table I—Equation (3)):

$$\Delta\psi = \frac{A_L^{\text{md}}}{wue\ r\ g_{\text{root-xylem}}} \cdot 1. \quad (2)$$

Under non-limiting light yet water-stressed conditions  $A_L^{\text{md}} = V l f(\psi_x)$ , with  $f(\psi_x)$  the stomatal closure in response to water stress, that is photosynthesis is limited by water stress and stomata closure. The maximum diurnal drop of xylem water potential thus simplifies to:

$$\Delta\psi = \frac{V\ l}{wue\ r\ g_{\text{root-xylem,max}}} \cdot 1. \quad (3)$$

We linearize the xylem embolism response instead of the full Weibull function (see Figure 2), with full conductivity loss at  $\psi_x = \psi_{\text{crit}}$  and no cavitation above  $\psi_x = \psi_e$  (which are derived from the full Weibull function). When there is stress ( $\psi_x > \psi_e$ ) the xylem percent loss conductivity *PLC* is simply:

$$PLC = 100 \left( 1 - \frac{\psi_x - \psi_{\text{crit}}}{\psi_e - \psi_{\text{crit}}} \right). \quad (4)$$

This can be used to define the maximum diurnal percentage loss of conductivity  $PLC_{\text{max}}$  using Equation (2):

$$PLC = 100 \left( 1 - \frac{1}{2} \frac{\psi_s' - \Delta\psi - \psi_{\text{crit}}}{\psi_e - \psi_{\text{crit}}} \right) \quad (5)$$

as well as the safety margin (SM) to the critical transpiration  $E_{\text{crit}}$  (Sperry *et al.*, 1998), which is defined as the maximum transpiration rate:

$$T = g_{\text{root-xylem,max}} \frac{\psi_x - \psi_{\text{crit}}}{\psi_e - \psi_{\text{crit}}} (\psi_s' - \psi_x)$$

for a given soil water potential and which is found at  $\psi_x = (\psi_s' + \psi_{\text{crit}})/2$ :

$$E_{\text{crit}} = g_{\text{root-xylem,max}} \frac{1}{4} \frac{(\psi_s' - \psi_{\text{crit}})}{\psi_e - \psi_{\text{crit}}}. \quad (6)$$

The safety margin (Sperry *et al.*, 1998) is then simply defined as:

$$SM = 1 - \frac{T}{E_{\text{crit}}} = 1 - 4 \frac{(\psi_s' - \Delta\psi - \psi_{\text{crit}})^2}{(\psi_s' - \psi_{\text{crit}})^2}, \quad (7)$$

where the diurnal water drop  $\Delta\psi$  linearly increases with photosynthetic flux  $A_L^0$ , root:shoot ratio and stress-free xylem resistivity  $1/g_{\text{root-xylem,max}}$  (see Equation (3)).

The safety margin, *SM*, rapidly decreases with soil water potential for piñons, as seen in Figure 10. It also decreases strongly during the day with the diurnal drop in xylem water potential. Hence, reduction of the dangerous xylem and leaf water potential diurnal drop (isohydric response) is required for piñon survival to droughts. The reduction of the safety margin is also linked with a larger drop in xylem hydraulic conductivity and a higher critical transpiration. In other words, for piñons, an improved safety margin is achieved through the reduction of  $\Delta\psi$  with: increased root:shoot (r:l) ratio, increased maximum whole-plant hydraulic conductance  $g_{\text{root-xylem,max}}$ , increased water-use efficiency and stomatal regulation to reduce evaporative demand. The safety margin of junipers, on the other hand, is not particularly sensitive to the diurnal drop of xylem water

SURVIVAL STRATEGIES OF HYDRAULIC FAILURE AND CARBON STARVATION

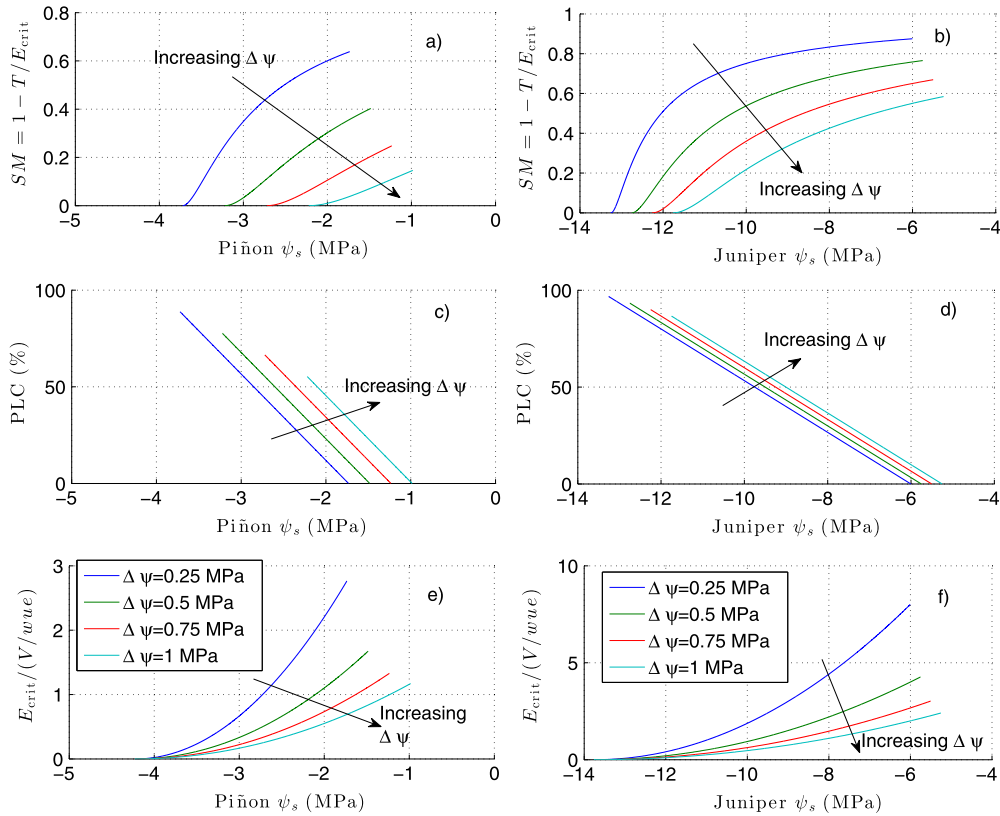


Figure 10. (top row) Safety margin (SM)—dimensionless, (middle row) percent loss of conductivity (PLC) and normalized critical transpiration  $E_{crit}$  as a function of soil water potential  $\psi_s$ , and diurnal peak in xylem water potential  $\Delta\psi$  for piñons (left-hand side) and junipers (right-hand side).

potential (Figure 10) so that stomatal regulation only provides marginal benefit to avoid desiccation, consistent with little stomatal regulation and an anisohydric behaviour (Tables II and III).

Decreased wood density in piñons increases specific hydraulic conductivity (Bucci *et al.*, 2004). On the other hand, wood density is also related to the shape of the vulnerability curve: increased wood density is often achieved by the narrowing of tracheid diameter (Pittermann *et al.*, 2006), which is negatively correlated with cavitation risk (Linton *et al.*, 1998). Because hydraulic conductance is inversely proportional to tree height, cavitation risks also increase with tree height and with decreased sapwood to

crown area ratio. Piñons with their more conductive xylem can mitigate xylem and leaf water potential drop (as seen in equation (3)) consistent with a isohydric behaviour.

Rooting depth

The time spent in stage 1 and stage 2 as well as the time to hydraulic failure increase linearly with rooting depth  $z_r$  for both species. Yet increased rooting depth is more beneficial for junipers than for piñons. A 1-m increase in rooting depth typically doubles the time to hydraulic failure for junipers. An increased rooting depth is beneficial for both species because it reduces hydraulic failure through

Table II. General parameters used in this study.

Name	Symbol	Units	Value	Source
Sand fraction*		—	0.54	Plaut <i>et al.</i> (2012)
Clay fraction		—	0.06	Plaut <i>et al.</i> (2012)
Potential at field capacity	$\psi_{fc}$	MPa	-0.3	Manfreda <i>et al.</i> , (2009)
Potential at residual soil moisture	$\psi_h$	MPa	-10	Manfreda <i>et al.</i> , (2009)
Potential evaporation	$E_p$	$W m^{-2}$	500	(Observations)
Incident photosynthetically active radiation	$L_0$	W PAR	669	(Observations)
Threshold for definition of cavitation	$\varepsilon$	%	5	

\*Denotes input parameters of allometric relationships.

Table III. Parameters used in this study for piñons and junipers.

Name	Symbol	Units	Value for piñon	Value for juniper	Source
Root:shoot ratio*	$r/l$	$m^2 m^{-2}$	0.3	1	West <i>et al.</i> (2008) (Observations)
Stem diameter at breast height*	$D$	cm	21.71 (on 50 piñons)	31.64 (on 65 junipers)	Pittermann <i>et al.</i> (2006) (Observations)
Wood density*	$r_d$	$g cm^{-3}$	0.6	0.65	Dai <i>et al.</i> , (2003) (Observations)
Height scaling parameter	$H$	cm to m	0.5	0.5	(Observations)
Efficiency factor from moles of photons to moles of carbon	$\alpha$	$mol_{CO_2} (mol photons)^{-1}$	0.06	0.06	(Observations)
Specific leaf area	$SLA$	$m^2 kg^{-1}$	3.5	2.04	(Observations)
Leaf area parameter	$a_l$	cm to $m^2$	0.089	0.0773	(Observations)
Leaf area parameter	$b_l$	cm to $m^2$	1.92	1.69	(Observations)
Sapwood area parameter	$a_{sw}$	cm to $m^2$	$8.1901 \cdot 10^{-5}$	$8.1901 \cdot 10^{-5}$	(Observations)
Sapwood area parameter	$b_{sw}$	cm to $m^2$	1.73	1.39	(Observations)
Rooting depth*	$z_r$	m	2	2	Tuning parameter (Observations)
Crown diameter	$D_c$	m	$0.368 D^{0.822}$	$0.329 D^{0.759}$	Plaut <i>et al.</i> (2012) (Observations)
Conductivity loss parameter	$\psi_k$	MPa	-3.4	-11	Plaut <i>et al.</i> (2012) (Observations)
Conductivity loss parameter	$c_k$		4	3.85	Plaut <i>et al.</i> (2012) (Observations)
Maximum rate of carbon assimilation	$V$	$mmol_{CO_2} m^{-2} s^{-1}$	80	80	Calibration

\*Denotes main model parameters.

increased accessible soil water volume, which buffers the precipitation variability. The impact of deeper rooting depth on carbon starvation is only marginal despite the increase in carbon allocation required to build deeper roots.

### Water-use efficiency

Water-use efficiency (*wue*) increases nearly linearly the time to hydraulic failure and carbon starvation (not shown). Increased *wue* is more efficient at protecting junipers from hydraulic failure than piñons. During stage 2 transpiration/photosynthesis the increased *wue* is less beneficial for piñons whereas the response of both species to increased *wue* during stage 1 is relatively similar. Across many species, *wue* tends to increase with rising CO<sub>2</sub> based on FLUXNET observations (Keenan *et al.*, 2013). All other tree traits being similar and with similar precipitation patterns, our results suggest that such increased *wue* with CO<sub>2</sub> rise should increase tree-level resistance to droughts and should further favour the more anisohydric junipers.

## DISCUSSION

We have introduced a simplified SPAC model based on allometric relationships in order to emphasize the role of tree traits for drought survival while reducing the number of model parameters. Compared with previous models, the model is sufficiently simple to be tractable and to permit exploration of the parameter space and infer the role of the different traits on carbon starvation and hydraulic failure. Our findings emphasize the importance of simultaneously considering all tree traits to fully comprehend the survival strategies to drought. The interplay between water use efficiency, root:shoot ratio, leaf area index, maximum hydraulic conductivity, loss of hydraulic conductivity, maximum rate of carbon assimilation and specific leaf area index determines the overall resistance to drought either via hydraulic failure or carbon starvation. Insights based on only one of those traits could be misleading and give an incomplete picture of drought resistance. In particular we have highlighted the interdependence of different traits on plant survival (e.g. the relationship between root:shoot ratio, tree LAI and cavitation curve) and the need for an integrated approach. The model is also sufficiently simple so that it could be scaled up to the landscape level.

### Juvenile versus mature tree—allometry

The model results presented assumed that the piñon and juniper were mature trees with diameters corresponding to the mean value of target trees. We now investigate the effect of tree diameters on drought resistance. We use the tree distribution and means of tree diameters for flat, south- and north-facing slopes from measurements collected in 2006 before the drought experiment was set up. The north- and

south-facing slopes are a natural drought experiment because the net infiltration of precipitation and soil moisture storage are reduced compared to the flat surface and the south-facing slopes that have higher insulation.

Junipers have similar mean diameter and diameter distributions in the north-facing, south-facing and flat surfaces ( $p > 0.05$ ), as seen in Figure 11. The absence of slope differences and the relatively uniform distribution among trees below 30 cm diameter suggest that soil hydrology does not strongly impact the highly drought-resistant junipers. Varying tree diameter in our model further supported the negligible effect of drought on juniper, with long but decreasing time to hydraulic failure (Figure 12). Although potential changes in the frequency and duration of precipitation could affect the resilience of junipers, our model results from north- and south-facing slopes suggest that the population dynamics of junipers will not be drastically impacted (beside under major droughts), a finding that is also supported by the limited dead junipers observed in the field drought treatment (Plaut *et al.*, 2012, 2013).

In contrast to the even distribution of tree diameters in juniper, the distribution of piñons was noticeably different with large-diameter piñons overrepresented on slopes relative to the flat block ( $p < 0.05$ ), as seen in Figure 11. This observation emphasizes the strong sensitivity of piñons to changes in hydrology and precipitation characteristics. Smaller-diameter piñons are much more sensitive to hydraulic failure and carbon starvation (Figure 12) and died from carbon starvation in our model. This could

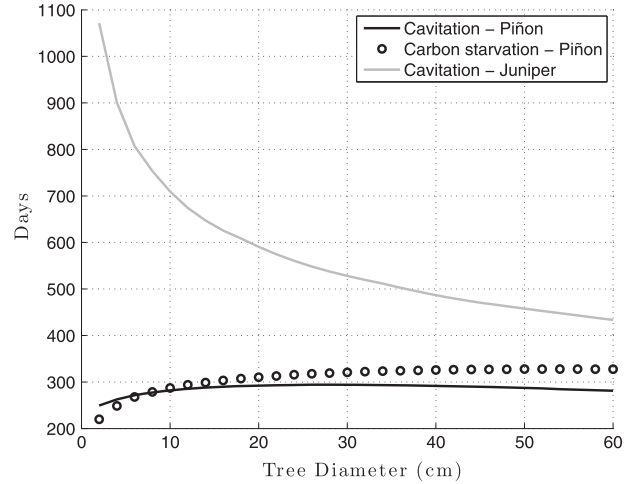


Figure 12. Sensitivity time to hydraulic failure and carbon starvation (defined as 0-crossover of NSC content—bottom right) to tree diameter  $D$ . Carbon starvation is outside the range of the figure and is thus not shown.

explain the preponderance of larger-trees over sloped surfaces with lower water content. Of course, smaller trees are more susceptible to competition from larger trees and recruitment may be favoured in flat areas (Floyd *et al.*, 2009); this is related to variation among species in their ability to germinate and develop a viable root system quickly. Recruitment in the drier-sloped terrains might be more episodic—in wet years—which could further narrow down the distribution. Our observations nonetheless support a pronounced sensitivity of smaller piñons to droughts.

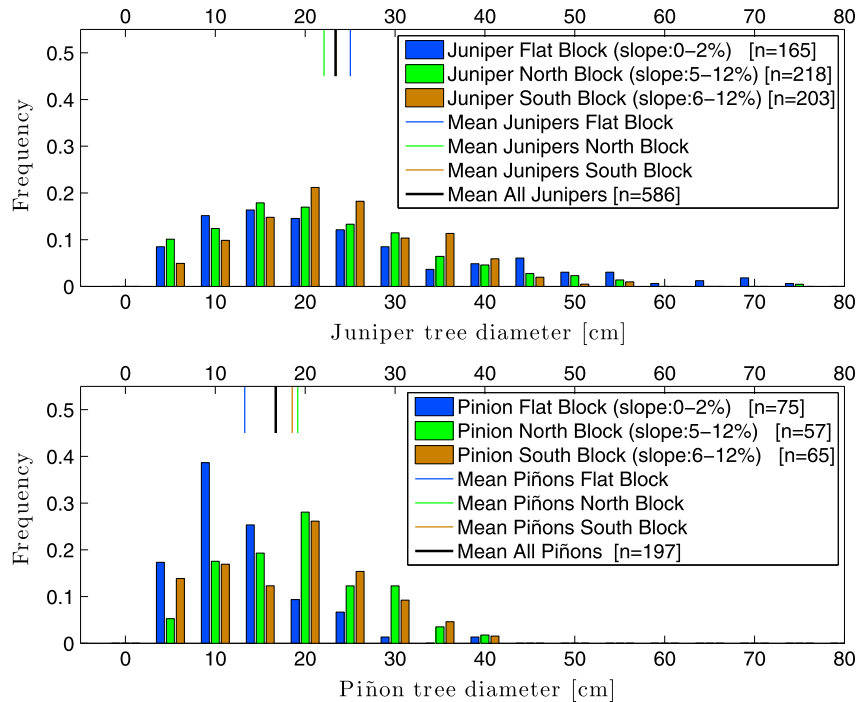


Figure 11. Histogram of observed juniper and piñon diameter at breast height on north-facing, south-facing and flat surfaces. The means are plotted as a line on top of the inset.

### Carbohydrate utilization and mobilization

The simplicity of the SPAC model described has inherent limitations. One of the main simplifications of the model is that carbon starvation is assumed to occur when the pool of carbon storage is reduced to a low value (2%). In reality the mechanism of carbon starvation may be more complicated because carbohydrate utilization and mobilization may be impeded at a given plant water status (Sala *et al.*, 2012; Mitchell *et al.*, 2012). The physiological mechanisms of drought-induced tree mortality are far from being resolved, and mechanisms of carbon starvation are still poorly understood and often times no clear pattern between carbohydrate utilization and mortality emerges (Sala 2010). The differentiation between starch and sugar pools may be important because depleted starch pools have been shown to be correlated with mortality (Marshall & Waring 1985; Adams *et al.*, 2009). Phloem transport failure may be another component of carbon starvation through phloem unloading to refill cavitated xylem tissues and lowering carbohydrate loading (Hölttä *et al.*, 2009) but the understanding of phloem transport and its coupling to xylem transport is still in its early stages even if important progresses have been made recently (Mencuccini & Hölttä 2009; Hölttä *et al.*, 2011; Nikinmaa *et al.*, 2012; Mencuccini *et al.*, 2013). Also in our model the LAI was not able to drop under drought to mitigate evaporative losses. The NSC storage was located in the roots and canopy, and we assumed that NSC in the roots could easily be mobilized when needed.

### CONCLUSIONS

A simplified soil–plant–atmosphere–continuum model of carbon starvation and hydraulic failure has been developed and tested against observations from a drought-manipulation study in a woodland dominated by piñon pine (*P. edulis*) and juniper trees (*J. monosperma*) in New Mexico. The model uses allometric relationships to reduce the number of parameters and to understand the mechanisms of carbon starvation and hydraulic failure. The model is sufficiently simple to highlight the role of the different traits on drought resistance.

For piñons, the number of days to hydraulic failure was relatively insensitive to the root:shoot ratio across a range of tree LAI. Higher root:shoot ratio however strongly decreased the days to carbon starvation. The model indicated that the time to hydraulic failure for juniper was much less sensitive to changes in root:shoot ratio than for piñon but was highly dependent on the tree LAI. In addition narrower tracheid diameter and narrower distribution of diameters, as observed in junipers, reduce the risk of hydraulic failure and carbon starvation.

Smaller-diameter piñons were more sensitive to hydraulic failure and carbon starvation than larger ones and often died from carbon starvation in our model. Smaller-diameter

junipers on the other hand were more prone to hydraulic failure and carbon starvation than larger trees.

The model presented here is a simplification of the complex and still poorly understood processes involved in carbon starvation and hydraulic failure but is an attempt at integrating the different factors (soil, hydrology, physiology, carbon and water budgets) controlling carbon starvation and hydraulic failure. Nonetheless the model provides insights into the effect of the different traits (leaf area index, root:shoot ratio, rooting depth and cavitation) as well as the role of age on survival to droughts. Future work will further use this model to better comprehend the differential factors of anthropogenic climate changes on plant survival to droughts. The trait-dependent representation of hydraulic failure and carbon starvation of this model is currently under development for implementation into a full-blown land surface model.

### ACKNOWLEDGEMENTS

The authors would like to thank Caroline Farrior for help with her model, Gabriel Katul, Paolo D'Odorico and Amilcare Porporato for discussions of our preliminary results. Collection of the experimental data used to test the model was supported by the Office of Science, United States Department of Energy and the National Science Foundation Long Term Ecological Research (LTER) program via the Sevilleta LTER.

### REFERENCES

- Adams HD, Guardiola-Claramonte M, Barron-Gafford GA, Villegas JC, Breshears DD, Zou CB, Troch PA, Huxman TE. 2009. Temperature sensitivity of drought-induced tree mortality portends increased regional die-off under global-change-type drought. *Proceedings of the National Academy of Sciences of the United States of America* **106**: 7063–7066.
- Albertson JD, Montaldo N. 2003. Temporal dynamics of soil moisture variability: 1. Theoretical basis. *Water Resources Research* **39**: 1–14.
- Allen, Craig D., Macalady AK, Chenchouni H, Bachelet D, McDowell N, Venetier M, Kizberger T, Rigling A, Breshears DD, Hogg EH, Gonzalez P, Fensham R, Zhang Z, Castro J, Demidova N, Lim JH, Allard G, Running SW, Semerci A, Cobb N. 2010 A global overview of drought and heat-induced tree mortality reveals emerging climate change risks for forests. *Forest Ecology and Management* **259**(4): 660–684.
- Anderegg WRL, Berry JA, Smith DD, Sperry JS, Anderegg LDL, and Field CB 2012. The roles of hydraulic and carbon stress in a widespread climate-induced forest die-off. *Proceedings of the National Academy of Science USA* **109**(1): 233–237. DOI: 10.1073/pnas.1107891109.
- Blasone R, Vrugt J, Madsen H, Rosbjerg D. 2008. Generalized likelihood uncertainty estimation (GLUE) using adaptive Markov Chain Monte Carlo sampling. *Advances in Water Resources* **630–648**.
- Bucci SJ, Goldstein G, Meinzer FC, Scholz FG, Franco AC, Bustamante M. 2004. Functional convergence in hydraulic architecture and water relations of tropical savanna trees: from leaf to whole plant. *Tree Physiology* **24**: 891–899.
- Brooks R, Corey A. 1964. Hydraulic properties of porous media. *Hydrol. Paper 3*, Colo. State Univ., Fort Collins, CO.
- Brutsaert W. 2005. *Hydrology*. Cambridge University Press 603p.
- Cochard H. 2002. A technique for measuring xylem hydraulic conductance under high negative pressures. *Plant, Cell and Environment* **25**: 815–819.

- Cochard H, Damour G, Bodet C, Tharwat I. 2005. Evaluation of a new centrifuge technique for rapid generation of xylem vulnerability curves. *Physiologia Plantarum* **124**: 410–418.
- D'Odorico P, Ridolfi L, Porporato A, Rodríguez-Iturbe I. 2000. Preferential states of seasonal soil moisture: the impact of climate fluctuations. *Water Resources Research* **36**: 2209–2219.
- Dai YJ, Zheng X, Dickinson RE, Baker I, Bonan GB, Bosilovich MG, Scott Denning A, Dirmeyer PA, Houser PR, Niu G, Oleson KW, Adam Schlosser C, Yang Z-L. 2003. The Common Land Model. *Bulletin of the American Meteorological Society*, **84**(8): 1013. DOI: 10.1175/BAMS-84-8-1013.
- Eagleson P. 1978a. Climate, soil, and vegetation. 1. Introduction to water balance dynamics. *Water Resources Research* **14**: 705–712.
- Eagleson P. 1978b. Climate, soil, and vegetation 2. The distribution of annual precipitation derived from observed storm sequences. *Water Resources Research* **14**: 713–721.
- Eagleson P. 1978c. Climate, soil, and vegetation 3. A simplified model of soil moisture movement in the liquid phase. *Water Resources Research* **14**: 722–730.
- Eagleson P. 1978d. Climate, soil, and vegetation 5. A derived distribution of storm surface runoff. *Water Resources Research* **14**: 741–748.
- Eagleson P. 1978e. Climate, soil, and vegetation, 6. Dynamics of the annual water balance. *Water Resources Research* **14**: 749–764.
- Edwards WRN, and Jarvis PG. 1982. Relations between water content, potential and permeability in stems of conifers. *Plant Cell Environ* **5**(4): 271–277. DOI: 10.1111/1365-3040.ep11572656.
- Farquhar GD, Sharkey TD. 1982. Stomatal conductance and photosynthesis. *Annual Review of Plant Physiology* **317–345**.
- Farquhar GD, Caemmerer von S, Berry JA. 2001. Models of photosynthesis. *Plant Physiology* **125**: 42–45.
- Farrior CE, Dybzinski R, Levin SA, Pacala SW. 2013. Competition for water and light in closed-canopy forests: a tractable model of carbon allocation with implications for carbon sinks. *The American Naturalist* **181**: 314–330.
- Fisher RA, Williams M, Do Vale RL, Da Costa AL, Meir P. 2006. Evidence from Amazonian forests is consistent with isohydric control of leaf water potential. *Plant, Cell and Environment* **29**: 151–165.
- Floyd ML, Clifford M, Cobb NS, Hanna D, Delph R, Ford P, & Turner D 2009. Relationship of stand characteristics to drought-induced mortality in three southwestern piñon—juniper woodlands. *Ecological Applications*, **19**(5), 1223–1230.
- Franks PJ, Drake PL, Froend RH. 2007. Anisohydric but isohydrodynamic: seasonally constant plant water potential gradient explained by a stomatal control mechanism incorporating variable plant hydraulic conductance. *Plant, Cell and Environment* **30**: 19–30.
- Gentine P, D'Odorico P, Lintner BR, Sivandran G, Salvucci G. 2012. Interdependence of climate, soil, and vegetation as constrained by the Budyko curve. *Geophysical Research Letters* **39**: L19404, DOI: 10.1029/2012GL053492.
- Hölttä T, Mencuccini M, Nikinmaa E. 2009. Linking phloem function to structure: analysis with a coupled xylem–phloem transport model. *Journal of Theoretical Biology* **259**: 325–337.
- Hölttä T, Mencuccini M, Nikinmaa E. 2011. A carbon cost-gain model explains the observed patterns of xylem safety and efficiency. *Plant, Cell and Environment* **34**: 1819–1834.
- Keenan TF, Hollinger DY, Bohrer G, Dragoni D, Munger JW, Schmid HP, Richardson AD. 2013. Increase in forest water-use efficiency as atmospheric carbon dioxide concentrations rise. *Nature* **499**: 324–327.
- Kumagai T, Porporato A. 2012. Strategies of a Bornean tropical rainforest water use as a function of rainfall regime: isohydric or anisohydric? *Plant, Cell and Environment* **35**: 61–71.
- Limousin J-M, Bickford CP, Dickman, LT, Pangle RE, Hudson PJ, Boutz AL, Gehres N, Osuna JL, Pockman WT, and McDowell NG. 2013. Regulation and acclimation of leaf gas exchange in a piñon–juniper woodland exposed to three different precipitation regimes. *Plant, Cell and Environment*, **36**(10), 1812–1825. DOI: 10.1111/pce.12089
- Linton M, Sperry J, Williams D. 1998. Limits to water transport in juniperus osteosperma and *Pinus edulis*: implications for drought tolerance and regulation of transpiration. *Functional Ecology* **12**: 906–911.
- Mahecha MD, Reichstein M, Carvalhais N, Lasslop G, Lange H, Seneviratne SI, Vargas R, Ammann C, Arain MA, Cescatti A, Janssens IA, Migliavacca M, Montagnani L, Richardson AD. 2010. Global convergence in the temperature sensitivity of respiration at ecosystem level. *Science* **329**(5993): 838–840.
- Manfreda S, Scanlon TM, Caylor KK. 2009. On the importance of accurate depiction of infiltration processes on modelled soil moisture and vegetation water stress. *Ecohydrology* **3**(2): 155–165. DOI: 10.1002/eco.79.
- Manzoni S, Vico G, Katul G, Porporato A, and Katul G. 2013. Advances in Water Resources. *Adv Water Resour*, **51**(C), 292–304. DOI: 10.1016/j.advwatres.2012.03.016
- Marshall JD, Waring RH. 1985. Predicting fine root production and turnover by monitoring root starch and soil temperature. *Canadian Journal of Forest Research* **15**: 791–800.
- McCulloh KA, Sperry JS, Adler FR. 2003. Water transport in plants obeys Murray's law. *Nature* **421**: 939–942.
- McCulloh KA, Sperry JS, Adler FR. 2004. Murray's law and the hydraulic vs mechanical functioning of wood. *Functional Ecology* **18**: 931–938.
- McCulloh KAK, Sperry JSJ. 2005. Patterns in hydraulic architecture and their implications for transport efficiency. *Tree Physiology* **25**: 257–267.
- McDowell N, Pockman WT, Allen CD, Breshears DD, Cobb N, Kolb T, Plaut JA, Sperry J, West A, Williams DG, Pockman WT, Allen CD, Breshears DD, Cobb N, Kolb T, Plaut J, Sperry J, West A, Williams DG, Yezzer EA. 2008. Mechanisms of plant survival and mortality during drought: why do some plants survive while others succumb to drought? *New Phytologist* **178**: 719–739.
- McDowell NG. 2011. Mechanisms linking drought, hydraulics, carbon metabolism, and vegetation mortality. *Plant Physiology* **155**: 1051–1059.
- McDowell NG, Fisher RA, Xu C, Domec JC, Hölttä T, Scott Mackay D, Sperry JS, Boutz A, Dickman L, Gehres N, Limousin JM, Macalady A, Martínez-Vilalta J, Mencuccini M, Plaut JA, Ogée J, Pangle RE, Rasse DP, Ryan MG, Sevanto S, Waring RH, Park Williams A, Yezzer EA, Pockman WT 2013. Evaluating theories of drought-induced vegetation mortality using a multimodel-experiment framework. *New Phytologist* **1–23**.
- McDowell NG, Beerling DJ, Breshears DD, Fisher RA, Raffa KF, Stitt M. 2011. The interdependence of mechanisms underlying climate-driven vegetation mortality. *Trends in Ecology & Evolution* **26**: 523–532.
- Meinzer FC, McCulloh KA. 2013. Xylem recovery from drought-induced embolism: where is the hydraulic point of no return? *Tree Physiology* **33**: 331–334.
- Meinzer FC, Johnson DM, Lachenbruch B, McCulloh KA, Woodruff DR. 2009. Xylem hydraulic safety margins in woody plants: coordination of stomatal control of xylem tension with hydraulic capacitance. *Functional Ecology* **23**: 922–930.
- Meinzer FC, Woodruff DR, Domec J-C, Goldstein G, Campanello PI, Gatti MG, Villalobos-Vega R. 2008. Coordination of leaf and stem water transport properties in tropical forest trees. *Oecologia* **156**: 31–41.
- Meinzer FC, Bond BJ, Warren JM, and Woodruff DR. 2005. Does water transport scale universally with tree size?. *Functional Ecology* **19**(4): 558–565. DOI: 10.1111/j.1365-2435.2005.01017.x.
- Mencuccini M, Hölttä T. 2009. The significance of phloem transport for the speed with which canopy photosynthesis and belowground respiration are linked. *New Phytologist* **185**: 189–203.
- Mencuccini M, Hölttä T, Sevanto S, Nikinmaa E. 2013. Concurrent measurements of change in the bark and xylem diameters of trees reveal a phloem-generated turgor signal. *New Phytologist* **1–12**.
- Mitchell PJ, O'Grady AP, Tissue DT, White DA, Ottenschlaeger ML, Pinkard EA. 2012. Drought response strategies define the relative contributions of hydraulic dysfunction and carbohydrate depletion during tree mortality. *New Phytologist* **197**: 862–872.
- Neufeld HSH, Grantz DAD, Meinzer FC, Goldstein GG, Crisosto GMG, Crisosto CC. 1992. Genotypic variability in vulnerability of leaf xylem to cavitation in water-stressed and well-irrigated sugarcane. *Plant Physiology* **100**: 1020–1028.
- Nikinmaa E, Hölttä T, Hari P, Kolari P, Makela A, Sevanto S, Vesala T. 2012. Assimilate transport in phloem sets conditions for leaf gas exchange. *Plant, Cell and Environment* **36**: 655–669.
- Pangle RE, Hill JP, Plaut JA, Yezzer EA, Elliot JR, Gehres N, McDowell NG, Pockman WT. 2012. Methodology and performance of a rainfall manipulation experiment in a piñon–juniper woodland. *Ecosphere* **3**: art 28.
- Phillips NG, Oren R, Licata J, Linder S. 2004. Time series diagnosis of tree hydraulic characteristics. *Tree Physiology* **879–890**.
- Pittermann J, Sperry JS, Wheeler JK, Hacke UG, Sikkema EH. 2006. Mechanical reinforcement of tracheids compromises the hydraulic efficiency of conifer xylem. *Plant, Cell and Environment* **29**: 1618–1628.

- Plaut JA, Wadsworth WD, Pangle RE, Yezpe EA, McDowell NG, Pockman WT. 2013. Reduced transpiration response to precipitation pulses precedes mortality in a piñon-juniper woodland subject to prolonged drought. *New Phytologist* DOI: 10.1111/nph.12392.
- Plaut JA, Yezpe EA, Hill J, Pangle RE, Sperry JS, Pockman WT, McDowell NG. 2012. Hydraulic limits preceding mortality in a piñon-juniper woodland under experimental drought. *Plant, Cell and Environment* **35**: 1601–1617.
- Pockman W, McDowell N 2006. Ecosystem-scale rainfall manipulation in a piñon-juniper forest at the Sevilleta National Wildlife Refuge, New Mexico: Meteorological Data (2006- ). Long Term Ecological Research Network. DOI: 10.6073/pasta/a053a821b84c51356730b4ee05a10e3f
- Pockman W, McDowell N 2013. Ecosystem-scale rainfall manipulation in a piñon-juniper forest at the Sevilleta National Wildlife Refuge, New Mexico: Volumetric Water Content (VWC) at 5 cm Depth Data (2006- ). Long Term Ecological Research Network. DOI: 10.6073/pasta/5441bd53a9b8c715c52bc04819da9f69
- Pockman W, McDowell N 2014. Ecosystem-scale rainfall manipulation in a Pinon-Juniper Woodland: VWC Profile Data (2009- ). Long Term Ecological Research Network. DOI: 10.6073/pasta/7c18af08dab5d604507163a548971bec
- Porporato A, Laio F, Ridolfi L, Rodríguez-Iturbe I. 2001. Plants in water-controlled ecosystems: active role in hydrologic processes and response to water stress—III. Vegetation water stress. *Advances in Water Resources* **24**: 725–744.
- Powell TL, Galbraith DR, Christoffersen BO, Harper A, Imbuzeiro H, Rowland L, Almeida S, Brando PM, da Costa ACL, Costa MH, Levine NM, Malhi Y, Saleska SR, Sotta E, Williams M, Meir P, and Moorcroft PR. 2013. Confronting model predictions of carbon fluxes with measurements of Amazon forests subjected to experimental drought. *New Phytologist* **200**(2): 350–365.
- Rodríguez-Iturbe I, Porporato A, Ridolfi L, Isham V, Cox DR. 1999. Probabilistic modelling of water balance at a point: the role of climate, soil and vegetation. *Proceedings of The Royal Society A-Mathematical Physical and Engineering Sciences* **455**: 3789–3805.
- Sala AA, Woodruff DR, Meinzer FCF. 2012. Carbon dynamics in trees: feast or famine? *Tree Physiology* **32**: 764–775.
- Sala AA. Physiological mechanisms of drought-induced tree mortality are far from being resolved. 2010. *Physiological mechanisms of drought-induced tree mortality are far from being resolved* **186**: 264–266.
- Salvucci GD. 1997. Soil and moisture independent estimation of stage-two evaporation from potential evaporation and albedo or surface temperature. *Water Resources Research* **33**: 111–122.
- Scholz FG, Bucci SJ, Goldstein G, Meinzer FC, Franco AC, Miralles-Wilhelm F. 2007. Biophysical properties and functional significance of stem water storage tissues in Neotropical savanna trees. *Plant, Cell and Environment* **30**: 236–248.
- Schultz HR 2003. Differences in hydraulic architecture account for near-isohydric and anisohydric behaviour of two field-grown *Vitis vinifera* L. cultivars during drought. *Plant, Cell and Environment*, **26**(8): 1393–1405. DOI: 10.1046/j.1365-3040.2003.01064.x
- Schwinning S, Ehleringer JR. 2001. Water use trade-offs and optimal adaptations to pulse-driven arid ecosystems. *Journal of Ecology* **464–480**.
- Secchi F, Zwieniecki MA. 2011. Sensing embolism in xylem vessels: the role of sucrose as a trigger for refilling, *Plant, Cell and Environment*, **34**: 514–524.
- Sevanto S, McDowell NG, Dickman LT, Pangle RE, Pockman WT. 2013. How do trees die? A test of the hydraulic failure and carbon starvation hypotheses. *Plant, Cell and Environment* **37**(1): 153–161.
- Sperry JS, Adler FR, Campbell GS, Comstock JP. 1998. Limitation of plant water use by rhizosphere and xylem conductance: results from a model. *Plant, Cell and Environment* **21**: 347–359.
- Sperry JS, Donnelly JR, Tyree MT. 1988. A method for measuring hydraulic conductivity and embolism in xylem. *Plant, Cell and Environment* **11**: 35–40.
- Sperry JS, Hacke UG, Oren R. 2002. Water deficits and hydraulic limits to leaf water supply. *Plant, Cell and Environment* **25**: 251–263.
- Tardieu F and Simonneau T. 1998. Variability among species of stomatal control under fluctuating soil water status and evaporative demand: modelling isohydric and anisohydric behaviours, **49**, 419–432.
- Tuzet A, Perrier A, Leuning R. 2003. A coupled model of stomatal conductance, photosynthesis and transpiration. *Plant, Cell and Environment* **26**: 1097–1116.
- Tyree MT, Sperry JS. 1989. Vulnerability of xylem to cavitation and embolism. *Annual Review of Plant Biology* **40**: 19–38.
- West AG, Hultine KR, Sperry JS, Bush SE, Ehleringer JR. 2008. Transpiration and hydraulic strategies in a piñon-juniper woodland. *Ecological Applications* **18**: 911–927.
- Williams M, Bond B, Ryan M. 2001. Evaluating different soil and plant hydraulic constraints on tree function using a model and sap flow data from ponderosa pine. *Plant, Cell and Environment* **24**: 679–690.
- Zhang Y, Meinzer FC, Qi J-H, Goldstein G, Cao K-F. 2012. Midday stomatal conductance is more related to stem rather than leaf water status in subtropical deciduous and evergreen broadleaf trees. *Plant, Cell and Environment* **36**: 149–158.

## SUPPORTING INFORMATION

Additional supporting information may be found in the online version of this article at the publisher's web site.